Efficient Single-Photon Detection with 7.7 ps Time Resolution for Photon-Correlation Measurements

Esmaeil Zadeh, Iman; Chang, Jin; Van Staaden, Yuri J.; Swens, Jeroen P.E.; Dobrovolskiy, Sergiy; Schaart, Dennis R.; Pereira, Silvania F.; Zwiller, Val; Dorenbos, Sander N.; More Authors

DOI
10.1021/acsphotonics.0c00433

Publication date
2020

Document Version
Final published version

Published in
ACS Photonics

ACS Photonics

pubs.acs.org/journal/apchd5

Article

Efficient Single-Photon Detection with 7.7 ps Time Resolution for Photon-Correlation Measurements

Iman Esmaeil Zadeh,*,§ Johannes W. N. Los,§ Ronan B. M. Gourgues, Jin Chang, Ali W. Elshaari, Julien Romain Zichi, Yuri J. van Staaden, Jeroen P. E. Swens, Nima Kalhor, Antonio Guardiani, Yun Meng, Kai Zou, Sergiy Dobrovolskiy, Andreas W. Fognini, Dennis R. Schaart, Dan Dalacu, Philip J. Poole, Michael E. Reimer, Xiaolong Hu, Silvania F. Pereira, Val Zwiller, and Sander N. Dorenbos

Cite This: *ACS Photonics* 2020, 7, 1780−1787

Read Online

ACCESS | Metrics & More | Article Recommendations | Supporting Information

ABSTRACT: A broad range of scientific and industrial disciplines require precise optical measurements at very low light levels. Single-photon detectors combining high efficiency and high time resolution are pivotal in such experiments. By using relatively thick films of NbTiN (8−11 nm) and improving the pattern fidelity of the nanostructure of the superconducting nanowire single-photon detectors (SNSPD), we fabricated devices demonstrating superior performance over all previously reported detectors in the combination of efficiency and time resolution. Our findings prove that small variations in the nanowire width, in the order of a few nanometers, can lead to a significant penalty on their temporal response. Addressing these issues, we consistently achieved high time resolution (best device 7.7 ps, other devices ∼10−16 ps) simultaneously with high system detection efficiencies (80−90%) in the wavelength range of 780−1000 nm, as well as in the telecom bands (1310−1550 nm). The use of thicker films allowed us to fabricate large-area multipixel devices with homogeneous pixel performance. We first fabricated and characterized a 100 × 100 μm^2 16-pixel detector and showed there was little variation among individual pixels. Additionally, to showcase the power of our platform, we fabricated and characterized 4-pixel multimode fiber-coupled detectors and carried out photon-correlation experiments on a nanowire quantum dot resulting in $g^2(0)$ values lower than 0.04. The multipixel detectors alleviate the need for beamsplitters and can be used for higher order correlations with promising prospects not only in the field of quantum optics, but also in bioimaging applications, such as fluorescence microscopy and positron emission tomography.

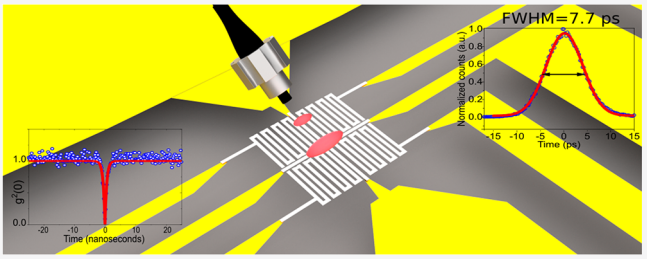

KEYWORDS: *superconducting nanowire single-photon detector, high time resolution, multipixel detectors, photon correlation, quantum optics*

SNSPDs have already pushed the limits in several fields such as CMOS testing,[1] biomedical imaging,[2] laser ranging,[3] and quantum communication.[4,5] These detectors have unparalleled performance: high efficiency (>90%),[6−8] time resolution (<3 ps for a short nanowire section[9] and <15 ps for complete efficient detectors[8,10]), and count-rate.[11] Yet, for studying the fast phenomena in chemistry, biology, and physics, efficient detectors with better timing jitter are required. Although direct high time-resolution measurements are possible, for example, with streak cameras, they suffer from low detection efficiencies, typically <10%, high dark count rates, and are limited to viewing a narrow time window;[12,13] moreover, they are bulky and costly. Meanwhile, the fiber-coupled SNSPDs allow for a cost-efficient integration of many high performance detectors in a single cryostat. Here we demonstrate SNSPDs made of relatively thick NbTiN films with superior time resolution and high efficiencies. Moreover, we show large area sensors using arrays of SNSPDs with minimal variation in performance over the array. In addition to optical imaging applications, this technology could be used to read-out fast scintillators, potentially enabling the detection of ionizing radiation with unprecedented time resolution, which is of great interest for time-of-flight positron emission tomography.[14] We showcase our platform by carrying out photon-correlation measurements using a multipixel multimode fiber-coupled detector.

We fabricate our detectors from sputtered NbTiN films on top of a SiO_2/Au cavity or a distributed Bragg reflector. To achieve the highest possible absorption in the superconducting layer, increasing the critical current and reducing kinetic

Received: March 17, 2020
Published: June 10, 2020

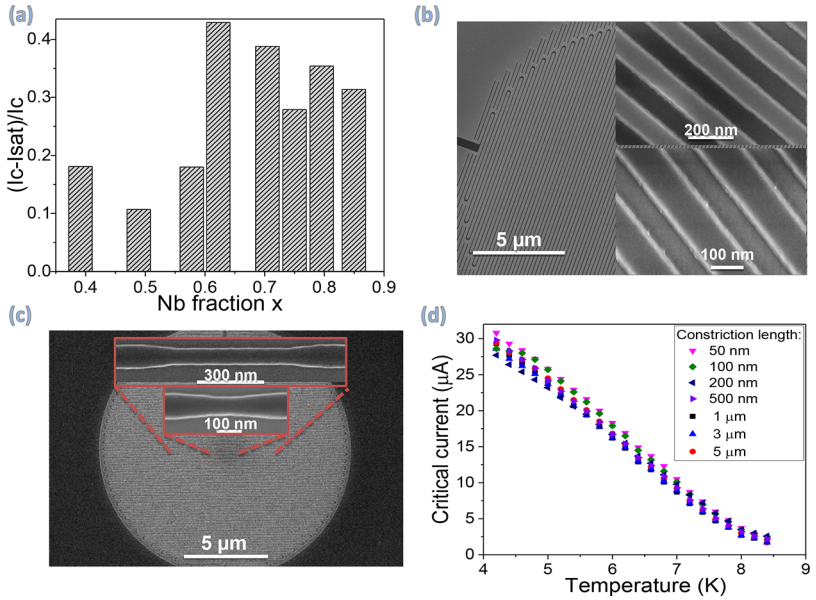

Figure 1. (a) Saturation of internal efficiency for sputtered, 9 nm thick, films of $Nb_xTi(1-x)N$ vs their Nb fraction at 830 nm. (b) SEM images of devices fabricated and optimized for the wavelength range of 800−900 nm. Top and bottom insets show devices with filling factor of ∼0.55 and 0.6, respectively. (c) Meander with a short constricted region. The main nanowire has a width of 100 nm and the width in the constriction region is 70 nm. The constriction length varies from 50 to 5000 nm and is always a straight section (not including bends). (d) Critical currents of devices described in (c) vs temperature. No significant change of critical currents was observed when changing the constriction length.

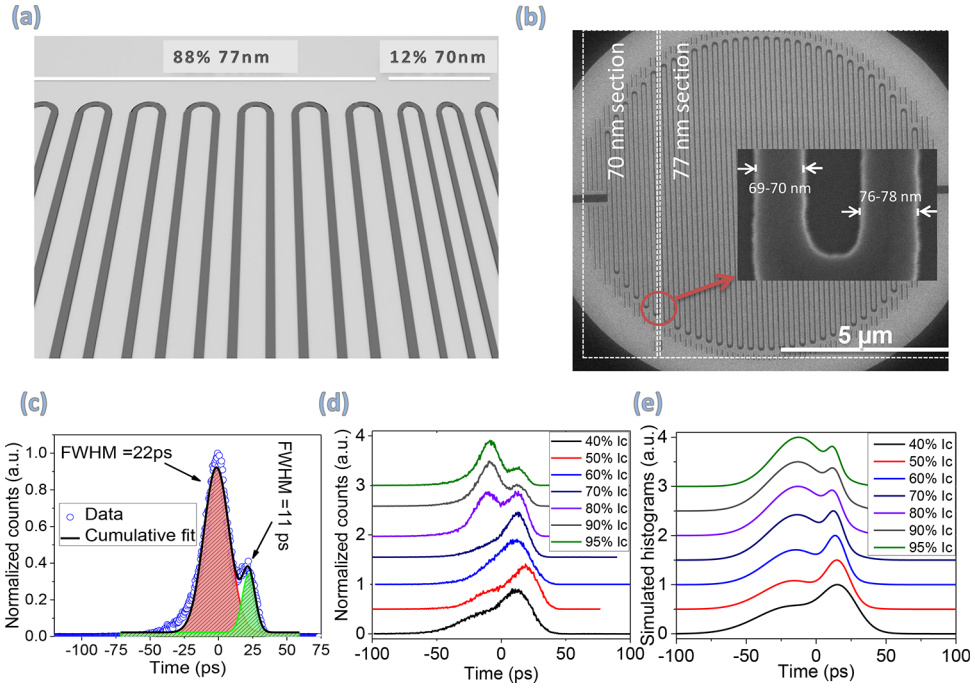

Figure 2. (a) Schematic illustration of a two-section SNSPD, having ∼12% (of its area) 70 nm nanowire width and ∼88% a width of 77 nm. (b) SEM image of a two section SNSPD. The inset shows a magnified high resolution SEM of the transition between 70 and 77 nm. The measured values were in good agreement with the design (also see Supporting Information for more SEM images). (c) Time jitter for the two-section SNSPD at a bias current equivalent to 95% of critical current. Two distinct peaks can be observed, which correspond to the two different meander sections. (d) Time jitter measurements for the same detector at various bias currents. It can be observed that, at lower biases, the detections mostly occur in the 70 nm section (higher internal saturation), while at higher biases it is dominated by the 77 nm section (larger surface area). This difference depends on the degree of saturation of each section. (e) Simulated correlation histograms at different bias currents.

inductance (and, hence, the deadtime), thicker films are desirable.[8] On the other hand, increasing the film thickness leads to a higher energy gap[15] and possible reduction of the kinetic energy of the quasiparticles due to less available energy following an excitation. Therefore, for such films, it is challenging to reach saturation of the internal efficiency, and hence, both the material properties of the film and the fabrication uniformity of the SNSPD nanowire meander have to be controlled.

https://dx.doi.org/10.1021/acsphotonics.0c00433
ACS Photonics 2020, 7, 1780−1787

FABRICATION AND CHARACTERIZATION

Magnetron sputtering was used to deposit the films, and similar to ref 16, we varied the sputtering parameters to achieve both high current and saturation of internal efficiency at the wavelength of 820 nm (we also optimized films and fabricated high performance devices optimized for the telecom wavelength range, see Supporting Information). Figure1a represents, similar to ref 16, the measured internal efficiency (the saturation plateau, $\frac{I_c - I_{sat}}{I_c}$) for detectors made from 9 nm thick films with different partial Nb contents. As it can be observed, all detectors with different Nb fractions show a saturation plateau, therefore, to enhance the signal-to-noise ratio and, hence, the timing jitter, we based our choice on the films that provided the highest critical current density and highest sheet resistance. All devices, unless mentioned, are fabricated from films with a Nb partial ratio of 0.85 ($Nb_{0.85}Ti_{0.15}N$). This composition yields detectors which not only have a high critical current density and a long saturation plateau (at the studied wavelength), but also can be operated at higher temperatures[17] and are compatible with large scale integrated nanophotonics.[18] We optimized our fabrication recipe and fabricated detectors with high uniformity. High-resolution SEM images of sample devices are shown in Figure1b.

Localized inhomogeneities are known to limit the critical current of SNSPDs made out of thin crystalline films (such as NbN and NbTiN).[19] We investigate whether the inhomogeneities can also affect our thicker NbTiN films by embedding short constrictions in the meandering detector, as shown in Figure1c. The main SNSPD meander had a width of 100 nm and the constriction was 70 nm wide. The length of this constriction was varied from 50 nm to 5 μm (always a straight section wire with no bends), and we measured their critical currents at several temperatures in the range of 4.2 to 8.5 K (Figure1d). We did not observe any significant degradation of critical current with the increase of constriction length. Furthermore, many of our fabricated shorter SNSPDs (~400 μm long) and longer SNSPDs (~4 mm long) showed similar critical currents.

It has been shown that local variation of nanowire width can influence the time resolution of SNSPDs.[20] To investigate the relevance of these local variations on the time resolution of our devices, we fabricate and characterize SNSPDs sectioned in two regions with different nanowire widths. Figure 2a is an illustration of such a two-sectioned SNSPD and Figure 2b shows an SEM image of a fabricated device with 70 and 77 nm wide sections. We designed the device so that the length of 77 nm wide section is about ~7.7× longer than the 70 nm wide section. The ratio between the length of different sections was experimentally chosen to signify the influence of widths variation and also the change in the profile of time response with respect to the bias current. We measure the SNSPD jitter by correlating the SNSPD pulses (start signal) with that of a pulsed laser (1060 nm, 5.08 ps, 48.6 MHz) as stop signal, shown in Figure 2c. Two distinct peaks can be observed, corresponding to the two different meander sections. We ascribe the peak on the right side to the 70 nm wide section because of its higher resistance which leads to faster rise time and hence earlier start signal. The fast rise time also leads to a narrower distribution since noise jitter is inversely proportional to the slope. The left side peak is ascribed to the 77 nm wide section which has the lower resistance and hence the late start signal. We also investigated the temporal profile of detection events as a function of bias current, as shown in Figure 2d.

To better understand the bias-current-dependent histograms of our two-section device, we numerically simulated these histograms, including electronic-noise-induced timing jitter,[21,22] geometric timing jitter,[23] and inhomogeneity-induced timing jitter,[24] see Supporting Information for details. As presented in Figure 2e, the simulated histograms show the features of double peaks that were also observed experimentally (Figure 2d). The system detection efficiency of each section determines the area under each peak and, therefore, is the major factor affecting the amplitude of each. As the system detection efficiency of the two sections both vary with the bias current, the relative areas of these two peaks also vary as a function of the bias current. The separation between the two peaks is the difference in time delays. We see that the simulated separations between the two peaks are larger than the measured results; so that at low bias level, two distinct peaks are obtained in simulation, as opposed to a main peak with a shoulder as observed experimentally. This discrepancy is mainly due to the fact that simulated leading edges of these time-domain pulses do not perfectly match the experimental results (see Supporting Information).

Nanofabrication of SNSPDs can introduce imperfections; the nanowire width may vary along the meander for a number of systemic and fabrication issues. A common factor is the proximity effect during electron beam lithography. The proximity effect can cause center areas of the detector to have a wider or narrower width (depending on the tone, thickness, and chemistry of the ebeam resist as well as the properties of the substrate, see Supporting Information for examples of proximity effect simulations), resulting in a similar behavior to that of Figure 2c. However, due to the limitations of the experimental setups, it is not always possible to resolve the peaks, yet we observed two distinct peaks in the temporal response of devices with a width difference as low as 2 nm (Supporting Information). It should be noted that if the device has more gradual widths variations (which is plausible considering the profile of proximity effects), instead of distinct peaks, one would expect a single broad peak. Proximity effects can be accounted and compensated for, however, it requires simulation, optimization, and verification for each single pattern, resist, and every electron beam lithography system. As our simulation suggests (Supporting Information), and from the literature,[25] it is possible to significantly reduce the PE using thinner ebeam resists. We tuned the resist thickness (for negative tone, 25−30 nm XR1541, and for positive tone 90−100 nm PMMA/AR-P 6200.04), the reactive ion etching chemistry (12.5 sccm SF_6, 3.4 sccm O_2, and a process pressure of ~4 μbar), and etching power and time (50 W and 45 s), and fabricated 70−100 nm wide nanowires made out of 10−13 nm thick films. The resulting detectors showed saturated internal efficiency in the wavelength range of 400−1064 nm. Note that the top section of the film has 0.5−1.5 nm oxidized layer,[26] preventing it from further oxidation. For high efficiency and high time resolution telecom detectors we used slightly thinner films (8.5−9.5 nm). For all fiber-coupled devices, unless otherwise clearly stated, the nanowire width and filling factor were 70 nm and 0.5, respectively.

For the measurement of high performance detectors, we packaged and characterized the detectors in a standard setup similar to ref 8. For efficiency measurements, at each wavelength we adjusted the input power to 10 nW and then

https://dx.doi.org/10.1021/acsphotonics.0c00433
ACS Photonics 2020, 7, 1780−1787

attenuated it by 50 dB, setting an input photon flux in the range of 200−800 K counts/s for visible to telecom wavelength range. For jitter measurements at low photon fluxes, we used a pico-second pulsed laser (same laser as was used for characterization of two-section detectors), and we kept the detector count-rate in the range of 60−100 K count/s. Figure3a and b present the efficiency and jitter measurement

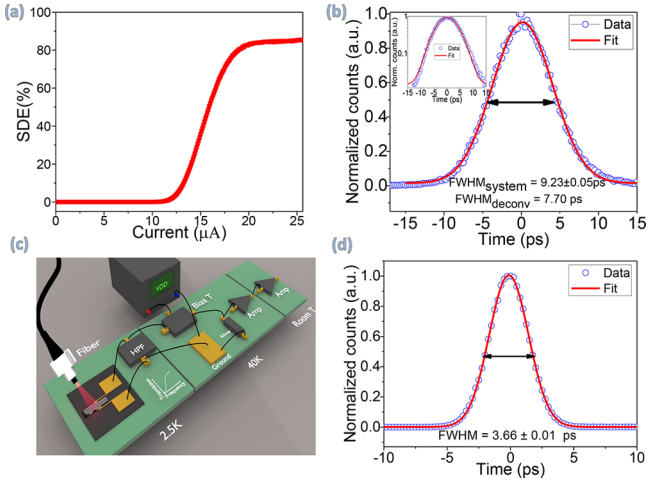

Figure 3. (a) Efficiency vs bias current for a detector at 915 nm, the peak efficiency is 85 ± 4.5%. (b) Jitter measurement for the same detector as part (a), the fwhm of the jitter, obtained from a Gaussian fit, is 9.23 ± 0.05 ps. Considering the duration of the laser pulses (5.08 ps) and neglecting the contribution from the correlator and photodiode (~2.5 ps), we obtain an SNSPD instrument response function of 7.70 ps (see Supporting Information). (c) An illustration of the SNSPD readout circuit used for high photon fluxes. (d) At higher photon fluxes using our new readout circuit, from the fit to the data, we calculated a system time resolution of 3.66 ± 0.01 ps (please note, this measurement was carried out on the device shown in S1(a)).

results for a detector optimized for the wavelength range of 880−950 nm (from a 10 nm thick film), respectively. For other wavelengths we achieved similar performance, see Supporting Information. We measured a system detection efficiency of >85(±5%) and system time resolution of 9.23 ± 0.05 ps (deconvoluted 7.70 ps, see Supporting Information). Other devices for this wavelength had SDE of 82−91.5% and time resolution of 9.5−15 ps (see Supporting Information). The inset in Figure3b is a logarithmic plot of the data and fit. On the left side of the jitter measurement data, a small asymmetry and deviation from the fit is observed. Besides originating from the nanowire width variation, this asymmetry could also be due to detection in the nanowire bends, as reported in ref 27. However, in comparison with ref 27, our degree of asymmetry is smaller, which most likely is explained by the nonuniform illumination of our device caused by the fact that the fiber coupled detector has a diameter larger than the mode field diameter of the optical fiber. As a result, the meander bends are not efficiently illuminated. The asymmetry was stronger when we flood illuminated the detectors in a free-space setup (in this case, bends were illuminated). To achieve the best time resolution, we triggered the correlator on the steepest part of the pulses rising edge. We also studied the effect of trigger level (varying it from 10% to 80%) on the value of the fwhm of detector jitter (see Supporting Information). An increase in the fwhm jitter can be observed, from 15.5 to 22.5 ps for a sample detector. This is likely to be caused by a reduced signal-to-noise ratio (slower rise time or higher noise level).

We also investigated the count-rate dependence of the jitter (see Supporting Information). We observed that, at low count rates (below 0.1 × laser repetition rate), the SNSPD time jitter exhibits a typical single Gaussian distribution. However, as the count-rate increases, other peaks start to appear in the distribution. The observation of these peaks can be explained by the fact that, when the bias recovery time of a SNSPD is longer than $\frac{1}{\text{laser rep. rate}}$, subsequent detection events take place with an underbiased detector, while detection events that are temporally further away would experience normal detection (similar to low count rate regime). Therefore, these different cases result in different rise time/signal levels, which consequently lead to multiple peaks in the jitter measurement.

Normally, SNSPDs under high excitation powers latch into the normal mode (they become normal with no recovery to the superconducting mode). By providing a low frequency path for the SNSPD current to ground, it is possible to operate detectors at higher powers. Moreover, by using high-bandwidth low-loss coax cables, a low jitter can be achieved. We use a high pass filter, as shown in Figure 3c, in series with the detector to allow for high power operation together with low jitter. The low-pass filter made it possible to operate the detector with higher power (1−10 nW). With higher intensity, we make sure that every single laser pulse is filled with several photons. Therefore, the rise time and signal level stay constant for all detection events, and the temporal distance between photons becomes shorter. Moreover, at these high powers, any SNSPD intrinsic/geometry contribution to the jitter is negligible, as only the fastest events trigger the correlator. To this end, the only limit we observed was the electrical noise and limited bandwidth of the amplifiers. The result of time jitter measurement with multiphoton excitation (>100 photons per pulse) is shown in Figure 3d, demonstrating a very high time-resolution of 3.66 ps (<3 ps after decoupling the contributions from the correlator and the photodiode, see Supporting Information).

QUANTUM CORRELATION WITH A MULTIPIXEL SNSPD

Many optical experiments in chemistry, biology, and material science deal with scattered light that cannot be efficiently collected and coupled into single mode optical fibers. Therefore, sensors with large active areas are required. SNSPDs with large active areas have gained attention in recent years, and several works on single pixel[28−31] and multipixel devices[32−34] have been reported. Compared to multipixel devices, single-pixel large-area devices are less complex and require only one readout channel. However, there is a price to pay, since many performance parameters of SNSPDs, such as deadtime and jitter and also fabrication yield, suffer as the device length is increased. Until now, these factors have limited the work of extending the size of single-pixel SNSPDs.

For multipixel SNSPD arrays, as the operation point and performance of individual pixels are usually not uniform, scaling these sensors also poses practical implementation challenges. Here we demonstrate, using our thick NbTiN films, multipixel arrays with small variations in performance of the pixels. Figure 4a shows SEM images of a fabricated 16 pixel SNSPD array covering an area of 100 × 100 μm^2 (pixel size 25

https://dx.doi.org/10.1021/acsphotonics.0c00433
ACS Photonics 2020, 7, 1780−1787

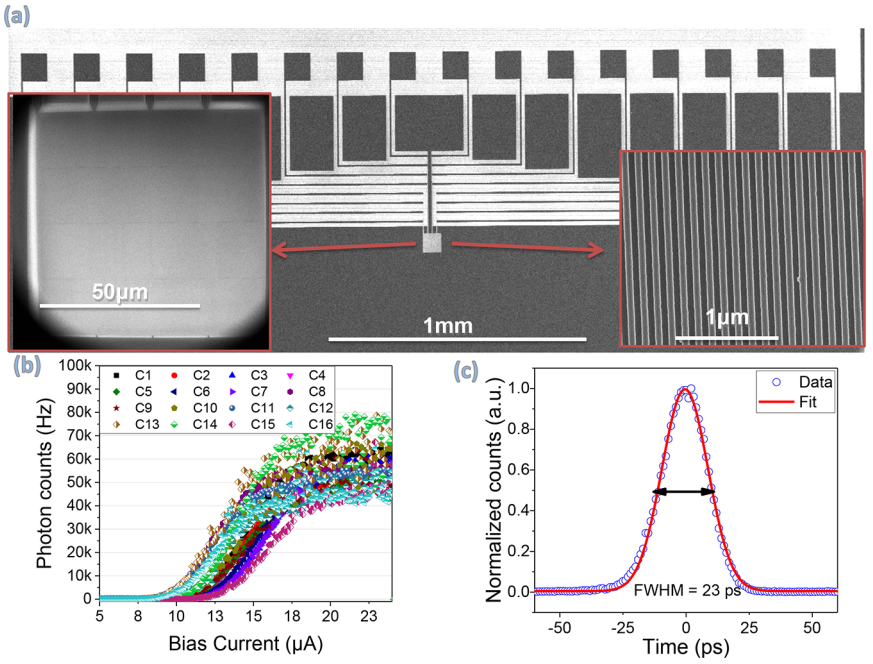

Figure 4. (a) SEM image of a fabricated 16 pixel SNSPD array covering an area of 100 × 100 μm^2 (pixel size 25 × 25 μm^2). The two insets show magnified images of the sensor array. (b) Photon count rate vs bias current for different pixels of the SNSPD array. The performance of different pixels is similar, and we attribute the small differences in pixel responses to the fact that the data was collected in two cool-down cycles (temperature and illumination variation). Nevertheless, for a bias current >20 μA, all pixels reach saturation of internal efficiency. (c) Timing jitter measurement for one of the pixels. The measured system jitter of 23 ps is >25× better if we only consider the reported geometrical jitter in other platforms.

× 25 μm^2). We measure the photon count rate versus bias current for different pixels of the SNSPD array using a flood-illumination setup at 670 nm. The results are presented in Figure 4b. It can be observed that the performance of all pixels are similar (for a bias current >20 μA, all pixels reach saturation of internal efficiency), and therefore, a much simpler biasing circuit can be used. We attribute the small differences in pixels responses to the fact that the data was collected in two cooldown cycles (cooldown 1: pixels 1−8, cooldown 2: pixels 9−16) and the temperature and illumination might had small variations (also within one cooldown there might be small variations in uniformity of illumination, see Supporting Information). The measured switching current, within each cooldown, for all but one pixel had a variation less than 2% (comparable to the precision of our biasing circuit). Only one pixel, due to a bonding issue, had an oscillatory behavior near the switching current, making it difficult to determine the exact switching current (the highest measured variation for this case was ∼10%). We also measured the time jitter for some pixels of the array, the results of one such measurement are provided in Figure 4c. The measured system jitter of 23 ps for a ∼4.46 mm long detector is >25× better than other platforms,[35−37] even considering only the geometrical jitter, which indicates that the electromagnetic field does not have as high a confinement in our platform as detectors made from thinner films (capacitive coupling of signal between the lines).

The multielement detectors are of particular interest in quantum optics, as they provide direct photon-correlation measurements with no need for spatially splitting the beam to different detectors. We carry out antibunching measurements using a four-pixel multimode fiber-coupled SNSPD (made from a 9.5 nm wide NbTiN film) on a semiconductor nanowire quantum dot. These sources have been extensively studied in the literature and have demonstrated promising performance in terms of clean emission spectra,[38] as entangled photon sources,[39] and for near-unity coupling to fibers.[40] We use a four-pixel multimode fiber-coupled SNSPD to carry photon-correlation measurements on the single photons generated by a nanowire quantum dot. SEM image of the detector is shown in Figure 5a with the ground pads (G), signal pads (S), and pixel labels (1, 2, 3, 4) highlighted in the figure. Our measurement setup is illustrated in Figure 5b, a cryogenically cooled source is excited using a CW laser (516 nm), and collected photons are filtered using a monochromator (Princeton Instrument Acton 2750) and are coupled to the detector through a graded index 50 μm fiber. We conduct photon-correlation measurements between different pixel pairs of the detector, and the results for three of these pairs are presented in Figure 5c (unprocessed data are available in the Supporting Information). The measured low value of $g^2(0)$, consistent or better than previously measured $g^2(0)$ on similar sources,[41] without using any beamsplitter demonstrates the usefulness and versatility of such detectors.

CONCLUSION

We demonstrated superconducting nanowire single-photon detectors (SNSPD), fabricated from NbTiN thick films, combining high time resolution and high efficiencies at the same time. The influence of fabrication imperfections on the time resolution of SNSPDs was studied, and it was revealed that a small variation in the order of a few nanometers can significantly influence the timing jitter. We showed that thicker films of NbTiN are less susceptible to small local material imperfections and are, therefore, a good candidate to serve as large active area, high-performance, photonic sensors. A multipixel detector was showcased as a quantum correlator

https://dx.doi.org/10.1021/acsphotonics.0c00433
ACS Photonics 2020, 7, 1780−1787

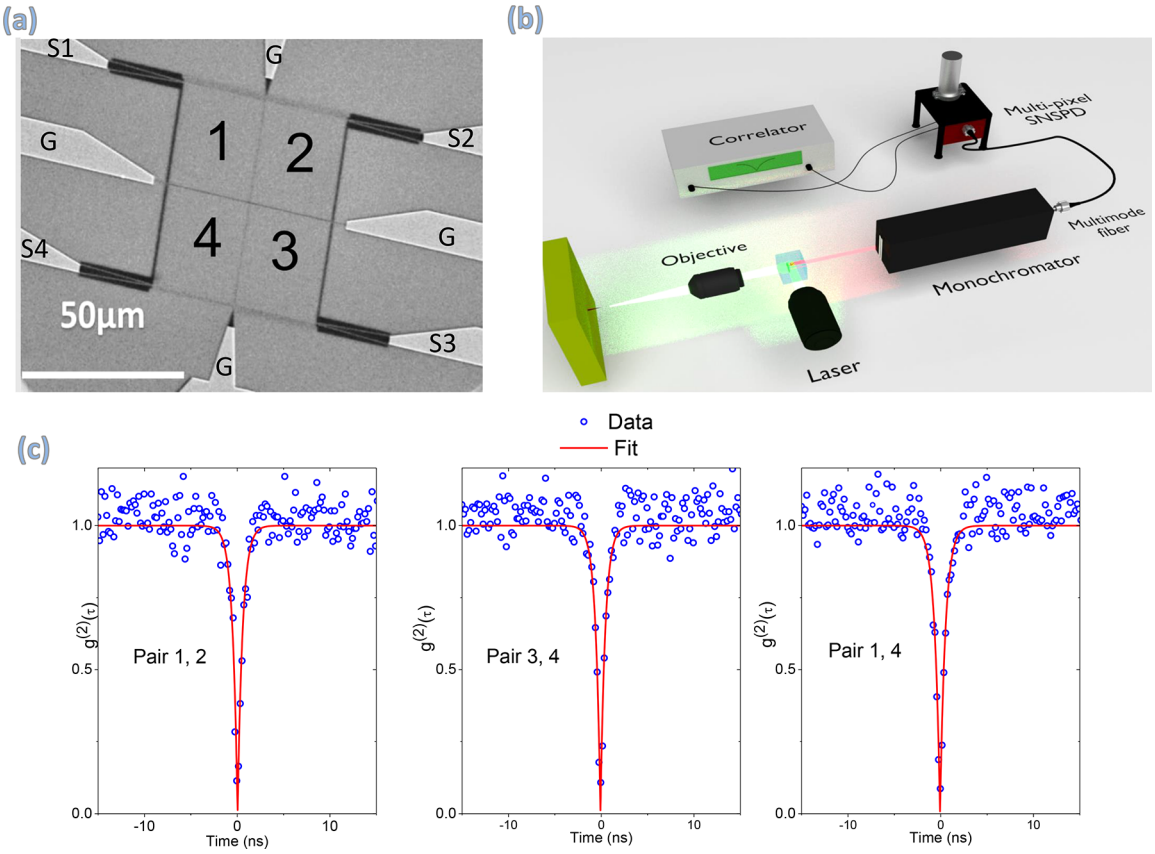

Figure 5. (a) SEM image of a fiber-coupled 4-pixel device covering an area of 50 × 50 μm^2. (b) Illustration of the photon antibunching measurement setup used to benchmark the 4-pixel detector. (c) Results of photon-correlation measurements with three out of six possible pixel pair combinations (complete data set can be found in Supporting Information). All pair combinations yield similar outcomes (depending on binning: a $g^2(0)$ between 0.03 and 0.1) while the fit at time 0 vanishes completely. The difference between the data and the fit is mainly due to timing jitter induced by a path-length difference in the monochromator (see Supporting Information).

in a Hanbury Brown and Twiss experiment without using a beamsplitter. The resulting low $g^2(0)$ demonstrates the potential of such devices not only in the field of quantum optics, but also in the fields such as fluorescence microscopy. Large-area multipixel SNSPDs are, furthermore, expected to have bright prospects in ultrafast optical and medical imaging applications.

■ ASSOCIATED CONTENT

Supporting Information

The Supporting Information is available free of charge at https://pubs.acs.org/doi/10.1021/acsphotonics.0c00433.

Additional examples of high-performance devices (S1) and information and simulations for detectors' time jitter (S2), as well as further data on multipixel devices (S3) (PDF)

■ AUTHOR INFORMATION

Corresponding Author

Iman Esmaeil Zadeh − *Optics Research Group, ImPhys Department, Faculty of Applied Sciences, Delft University of Technology, Delft 2628 CJ, The Netherlands; Single Quantum B.V., Delft 2628 CJ, The Netherlands;* orcid.org/0000-0002-3833-2508; Email: i.esmaeilzadeh@tudelft.nl

Authors

Johannes W. N. Los − *Single Quantum B.V., Delft 2628 CJ, The Netherlands*

Ronan B. M. Gourgues − *Single Quantum B.V., Delft 2628 CJ, The Netherlands*

Jin Chang − *Optics Research Group, ImPhys Department, Faculty of Applied Sciences, Delft University of Technology, Delft 2628 CJ, The Netherlands*

Ali W. Elshaari − *Quantum Nano Photonics Group, Department of Applied Physics, Royal Institute of Technology (KTH), Stockholm 106 91, Sweden;* orcid.org/0000-0002-7004-9665

Julien Romain Zichi − *Quantum Nano Photonics Group, Department of Applied Physics, Royal Institute of Technology (KTH), Stockholm 106 91, Sweden*

Yuri J. van Staaden − *Optics Research Group, ImPhys Department, Faculty of Applied Sciences, Delft University of Technology, Delft 2628 CJ, The Netherlands*

Jeroen P. E. Swens − *Optics Research Group, ImPhys Department, Faculty of Applied Sciences, Delft University of Technology, Delft 2628 CJ, The Netherlands*

Nima Kalhor − *Single Quantum B.V., Delft 2628 CJ, The Netherlands*

Antonio Guardiani − *Single Quantum B.V., Delft 2628 CJ, The Netherlands*

Yun Meng − *School of Precision Instrument and Optoelectronic Engineering, Tianjin University, Tianjin 300072, China; Key*

Laboratory of Optoelectronic Information Science and Technology, Ministry of Education, Tianjin 300072, China

Kai Zou − *School of Precision Instrument and Optoelectronic Engineering, Tianjin University, Tianjin 300072, China; Key Laboratory of Optoelectronic Information Science and Technology, Ministry of Education, Tianjin 300072, China*

Sergiy Dobrovolskiy − *Single Quantum B.V., Delft 2628 CJ, The Netherlands*

Andreas W. Fognini − *Single Quantum B.V., Delft 2628 CJ, The Netherlands*

Dennis R. Schaart − *Medical Physics and Technology, Radiation Science and Technology Department, Faculty of Applied Sciences, Delft University of Technology, Delft 2628 CJ, The Netherlands*

Dan Dalacu − *National Research Council of Canada, Ottawa, Ontario K1A 0R6, Canada*

Philip J. Poole − *National Research Council of Canada, Ottawa, Ontario K1A 0R6, Canada*

Michael E. Reimer − *Institute for Quantum Computing and Department of Electrical & Computer Engineering, University of Waterloo, Waterloo, Ontario N2L 3G1, Canada*

Xiaolong Hu − *School of Precision Instrument and Optoelectronic Engineering, Tianjin University, Tianjin 300072, China; Key Laboratory of Optoelectronic Information Science and Technology, Ministry of Education, Tianjin 300072, China;* orcid.org/0000-0002-5589-8538

Silvania F. Pereira − *Optics Research Group, ImPhys Department, Faculty of Applied Sciences, Delft University of Technology, Delft 2628 CJ, The Netherlands*

Val Zwiller − *Single Quantum B.V., Delft 2628 CJ, The Netherlands; Quantum Nano Photonics Group, Department of Applied Physics, Royal Institute of Technology (KTH), Stockholm 106 91, Sweden*

Sander N. Dorenbos − *Single Quantum B.V., Delft 2628 CJ, The Netherlands*

Complete contact information is available at: https://pubs.acs.org/10.1021/acsphotonics.0c00433

Author Contributions

[§]I.E.Z. and J.W.N.L. contributed equally to this work.

Funding

I.E.Z., A.W.E., V.Z., D.R.S., and Single Quantum B.v. acknowledge the supports from the ATTRACT project funded by the EC under Grant Agreement 777222. I.E.Z. acknowledges the support of Nederlandse Organisatie voor Wetenschappelijk Onderzoek (NWO), LIFT-HTSM (Project 680-91-202). R.B.M.G. acknowledges support by the European Commission via the Marie-Sklodowska Curie action Phonsi (H2020-MSCA-ITN-642656). A.W.E. acknowledges support from the Swedish Research Council (Vetenskapsrådet) Starting Grant (Ref 2016-03905). V.Z. acknowledges funding from the Knut and Alice Wallenberg Foundation Grant "Quantum Sensors", and support from the Swedish Research Council (VR) through the VR Grant for International Recruitment of Leading Researchers (Ref 2013-7152) and Research Environment Grant (Ref 2016-06122). Y.M., K.Z., and X.H. acknowledge support from the Natural Science Foundation of Tianjin City (19JCYBJC16900).

Notes

The authors declare no competing financial interest.

■ ACKNOWLEDGMENTS

The authors would like to thank Dr. Gabriele Bulgarini and Dr. Stephan Steinhauer for the fruitful discussions.

■ REFERENCES

(1) Zhang, J.; et al. Noninvasive CMOS circuit testing with NbN superconducting single-photon detectors. *Electron. Lett.* **2003**, *39*, 1086−1088.

(2) Pe'er, A.; Bromberg, Y.; Dayan, B.; Silberberg, Y.; Friesem, A. A. Broadband sum-frequency generation as an efficient two-photon detector for optical tomography. *Opt. Express* **2007**, *15*, 8760−8769.

(3) McCarthy, A.; Krichel, N. J.; Gemmell, N. R.; Ren, X.; Tanner, M. G.; Dorenbos, S. N.; Zwiller, V.; Hadfield, R. H.; Buller, G. S. Kilometer-range, high resolution depth imaging via 1560 nm wavelength single-photon detection. *Opt. Express* **2013**, *21*, 8904−8915.

(4) Yin, J.; Cao, Y.; Liu, S.-B.; Pan, G.-S.; Wang, J.-H.; Yang, T.; Zhang, Z.-P.; Yang, F.-M.; Chen, Y.-A.; Peng, C.-Z.; Pan, J.-W. Experimental quasi-single-photon transmission from satellite to earth. *Opt. Express* **2013**, *21*, 20032−20040.

(5) Vallone, G.; Dequal, D.; Tomasin, M.; Vedovato, F.; Schiavon, M.; Luceri, V.; Bianco, G.; Villoresi, P. Interference at the Single Photon Level Along Satellite-Ground Channels. *Phys. Rev. Lett.* **2016**, *116*, 253601.

(6) Marsili, F.; Verma, V. B.; Stern, J. A.; Harrington, S.; Lita, A. E.; Gerrits, T.; Vayshenker, I.; Baek, B.; Shaw, M. D.; Mirin, R. P.; Nam, S. W. Detecting single infrared photons with 93% system efficiency. *Nat. Photonics* **2013**, *7*, 210−214.

(7) Zhang, W. J.; You, L. X.; Li, H.; Huang, J.; Lv, C. L.; Zhang, L.; Liu, X. Y.; Wu, J. J.; Wang, Z.; Xie, X. M. NbN superconducting nanowire single photon detector with efficiency over 90% at 1550 nm wavelength operational at compact cryocooler temperature. *Sci. China: Phys., Mech. Astron.* **2017**, *60*, 120314.

(8) Esmaeil Zadeh, I.; Los, J. W. N.; Gourgues, R. B. M.; Steinmetz, V.; Bulgarini, G.; Dobrovolskiy, S. M.; Zwiller, V.; Dorenbos, S. N. Single-photon detectors combining high efficiency, high detection rates, and ultra-high timing resolution. *APL Photonics* **2017**, *2*, 111301.

(9) Korzh, B.; Zhao, Q.-Y.; Allmaras, J. P.; Frasca, S.; Autry, T. M.; Bersin, E. A.; Beyer, A. D.; Briggs, R. M.; Bumble, B.; Colangelo, M.; Crouch, G. M.; Dane, A. E.; Gerrits, T.; Lita, A. E.; Marsili, F.; Moody, G.; Pena, C.; Ramirez, E.; Rezac, J. D.; Sinclair, N.; Stevens, M. J.; Velasco, A. E.; Verma, V. B.; Wollman, E. E.; Xie, S.; Zhu, D.; Hale, P. D.; Spiropulu, M.; Silverman, K. L.; Mirin, R. P.; Nam, S. W.; Kozorezov, A. G.; Shaw, M. D.; Berggren, K. K. Demonstration of sub-3 ps temporal resolution with a superconducting nanowire single-photon detector. *Nat. Photonics* **2020**, *14*, 250−255.

(10) Wu, J.; You, L.; Chen, S.; Li, H.; He, Y.; Lv, C.; Wang, Z.; Xie, X. Improving the timing jitter of a superconducting nanowire single-photon detection system. *Appl. Opt.* **2017**, *56*, 2195−2200.

(11) Huang, J.; Zhang, W.; You, L.; Zhang, C.; Lv, C.; Wang, Y.; Liu, X.; Li, H.; Wang, Z. High speed superconducting nanowire single-photon detector with nine interleaved nanowires. *Supercond. Sci. Technol.* **2018**, *31*, 074001.

(12) Müller, A. M.; Bardeen, C. J. Using a Streak Camera to Resolve the Motion of Molecular Excited States with Picosecond Time Resolution and 150 nm Spatial Resolution. *J. Phys. Chem. C* **2007**, *111*, 12483−12489.

(13) Hamamatsu Photonics K.K. FESCA-100 fs streak camera. https://www.hamamatsu.com/eu/en/product/photometry-systems/streak-camera/fesca-100-femtosecond-streak-camera/index.html, accessed 19 April 2020.

(14) Seifert, S.; van Dam, H. T.; Schaart, D. R. The lower bound on the timing resolution of scintillation detectors. *Phys. Med. Biol.* **2012**, *57*, 1797−1814.

(15) Zhang, L.; Peng, W.; You, L. X.; Wang, Z. Superconducting properties and chemical composition of NbTiN thin films with different thickness. *Appl. Phys. Lett.* **2015**, *107*, 122603.

(16) Zichi, J.; Chang, J.; Steinhauer, S.; von Fieandt, K.; Los, J. W. N.; Visser, G.; Kalhor, N.; Lettner, T.; Elshaari, A. W.; Zadeh, I. E.; Zwiller, V. Optimizing the stoichiometry of ultrathin NbTiN films for high-performance superconducting nanowire single-photon detectors. *Opt. Express* **2019**, *27*, 26579−26587.
(17) Gourgues, R.; Los, J. W. N.; Zichi, J.; Chang, J.; Kalhor, N.; Bulgarini, G.; Dorenbos, S. N.; Zwiller, V.; Zadeh, I. E. Superconducting nanowire single photon detectors operating at temperature from 4 to 7 K. *Opt. Express* **2019**, *27*, 24601−24609.
(18) Gourgues, R.; Zadeh, I. E.; Elshaari, A. W.; Bulgarini, G.; Los, J. W. N.; Zichi, J.; Dalacu, D.; Poole, P. J.; Dorenbos, S. N.; Zwiller, V. Controlled integration of selected detectors and emitters in photonic integrated circuits. *Opt. Express* **2019**, *27*, 3710−3716.
(19) Gaudio, R.; op 't Hoog, K. P. M.; Zhou, Z.; Sahin, D.; Fiore, A. Inhomogeneous critical current in nanowire superconducting single-photon detectors. *Appl. Phys. Lett.* **2014**, *105*, 222602.
(20) O'Connor, J. A.; Tanner, M. G.; Natarajan, C. M.; Buller, G. S.; Warburton, R. J.; Miki, S.; Wang, Z.; Nam, S. W.; Hadfield, R. H. Spatial dependence of output pulse delay in a niobium nitride nanowire superconducting single-photon detector. *Appl. Phys. Lett.* **2011**, *98*, 201116.
(21) Zhao, Q.; Zhang, L.; Jia, T.; Kang, L.; Xu, W.; Chen, J.; Wu, P. Intrinsic timing jitter of superconducting nanowire single-photon detectors. *Appl. Phys. B: Lasers Opt.* **2011**, *104*, 673−678.
(22) You, L.; Yang, X.; He, Y.; Zhang, W.; Liu, D.; Zhang, W.; Zhang, L.; Zhang, L.; Liu, X.; Chen, S.; Wang, Z.; Xie, X. Jitter analysis of a superconducting nanowire single photon detector. *AIP Adv.* **2013**, *3*, 072135.
(23) Calandri, N.; Zhao, Q.-Y.; Zhu, D.; Dane, A.; Berggren, K. K. Superconducting nanowire detector jitter limited by detector geometry. *Appl. Phys. Lett.* **2016**, *109*, 152601.
(24) Cheng, Y.; Gu, C.; Hu, X. Inhomogeneity-induced timing jitter of superconducting nanowire single-photon detectors. *Appl. Phys. Lett.* **2017**, *111*, 062604.
(25) Li, P. A Review of Proximity Effect Correction in Electron-beam Lithography. *Arxiv preprint [cond-mat], arXiv: 1509.05169* **2015**, na.
(26) Cheng, R.; Guo, X.; Ma, X.; Fan, L.; Fong, K. Y.; Poot, M.; Tang, H. X. Self-aligned multi-channel superconducting nanowire single-photon detectors. *Opt. Express* **2016**, *24*, 27070−27076.
(27) Sidorova, M.; Semenov, A.; Hübers, H.-W.; Charaev, I.; Kuzmin, A.; Doerner, S.; Siegel, M. Physical mechanisms of timing jitter in photon detection by current-carrying superconducting nanowires. *Phys. Rev. B: Condens. Matter Mater. Phys.* **2017**, *96*, 184504.
(28) Liu, D.; Miki, S.; Yamashita, T.; You, L.; Wang, Z.; Terai, H. Multimode fiber-coupled superconducting nanowire single-photon detector with 70% system efficiency at visible wavelength. *Opt. Express* **2014**, *22*, 21167−21174.
(29) Li, H.; Zhang, L.; You, L.; Yang, X.; Zhang, W.; Liu, X.; Chen, S.; Wang, Z.; Xie, X. Large-sensitive-area superconducting nanowire single-photon detector at 850 nm with high detection efficiency. *Opt. Express* **2015**, *23*, 17301−17308.
(30) Wollman, E. E.; Verma, V. B.; Beyer, A. D.; Briggs, R. M.; Korzh, B.; Allmaras, J. P.; Marsili, F.; Lita, A. E.; Mirin, R. P.; Nam, S. W.; Shaw, M. D. UV superconducting nanowire single-photon detectors with high efficiency, low noise, and 4 K operating temperature. *Opt. Express* **2017**, *25*, 26792−26801.
(31) Chang, J.; Zadeh, I. E.; Los, J. W. N.; Zichi, J.; Fognini, A.; Gevers, M.; Dorenbos, S.; Pereira, S. F.; Urbach, P.; Zwiller, V. Multimode-fiber-coupled superconducting nanowire single-photon detectors with high detection efficiency and time resolution. *Appl. Opt.* **2019**, *58*, 9803−9807.
(32) Allman, M. S.; Verma, V. B.; Stevens, M.; Gerrits, T.; Horansky, R. D.; Lita, A. E.; Marsili, F.; Beyer, A.; Shaw, M. D.; Kumor, D.; Mirin, R.; Nam, S. W. A near-infrared 64-pixel superconducting nanowire single photon detector array with integrated multiplexed readout. *Appl. Phys. Lett.* **2015**, *106*, 192601.
(33) Allmaras, J. P.; Beyer, A. D.; Briggs, R. M.; Marsili, F.; Shaw, M. D.; Resta, G. V.; Stern, J. A.; Verma, V. B.; Mirin, R. P.; Nam, S. W.; Farr, W. H. Large-Area 64-pixel Array of WSi Superconducting Nanowire Single Photon Detectors. *Conference on Lasers and Electro-Optics*, CLEO, 2017; p JTh3E.7.
(34) Miyajima, S.; Yabuno, M.; Miki, S.; Yamashita, T.; Terai, H. High-time-resolved 64-channel single-flux quantum-based address encoder integrated with a multi-pixel superconducting nanowire single-photon detector. *Opt. Express* **2018**, *26*, 29045−29054.
(35) Kuzmin, A.; Doerner, S.; Sidorova, M.; Wuensch, S.; Ilin, K.; Siegel, M.; Semenov, A. Geometrical Jitter and Bolometric Regime in Photon Detection by Straight Superconducting Nanowire. *IEEE Trans. Appl. Supercond.* **2019**, *29*, 1−5.
(36) Santavicca, D. F.; Adams, J. K.; Grant, L. E.; McCaughan, A. N.; Berggren, K. K. Microwave dynamics of high aspect ratio superconducting nanowires studied using self-resonance. *J. Appl. Phys.* **2016**, *119*, 234302.
(37) Zhao, Q.-Y.; Santavicca, D. F.; Zhu, D.; Noble, B.; Berggren, K. K. A distributed electrical model for superconducting nanowire single photon detectors. *Appl. Phys. Lett.* **2018**, *113*, 082601.
(38) Dalacu, D.; Mnaymneh, K.; Lapointe, J.; Wu, X.; Poole, P. J.; Bulgarini, G.; Zwiller, V.; Reimer, M. E. Ultraclean Emission from InAsP Quantum Dots in Defect-Free Wurtzite InP Nanowires. *Nano Lett.* **2012**, *12*, 5919−5923.
(39) Versteegh, M. A. M.; Reimer, M. E.; Jöns, K. D.; Dalacu, D.; Poole, P. J.; Gulinatti, A.; Giudice, A.; Zwiller, V. Observation of strongly entangled photon pairs from a nanowire quantum dot. *Nat. Commun.* **2014**, *5*, 5298.
(40) Bulgarini, G.; Reimer, M. E.; Bouwes Bavinck, M.; Jons, K. D.; Dalacu, D.; Poole, P. J.; Bakkers, E. P. A. M.; Zwiller, V. Nanowire Waveguides Launching Single Photons in a Gaussian Mode for Ideal Fiber Coupling. *Nano Lett.* **2014**, *14*, 4102−4106.
(41) Zadeh, I. E.; Elshaari, A. W.; Jöns, K. D.; Fognini, A.; Dalacu, D.; Poole, P. J.; Reimer, M. E.; Zwiller, V. Deterministic Integration of Single Photon Sources in Silicon Based Photonic Circuits. *Nano Lett.* **2016**, *16*, 2289−2294.

https://dx.doi.org/10.1021/acsphotonics.0c00433
ACS Photonics 2020, 7, 1780−1787